Cell, Vol. 109, 913–923, June 28, 2002, Copyright ©2002 by Cell Press

Bacterial Adhesion to Target Cells Enhanced by Shear Force

Wendy E. Thomas,[1] Elena Trintchina,[2,6] Manu Forero,[1,3] Viola Vogel,[1,4] and Evgeni V. Sokurenko[2,5]
[1]Department of Bioengineering
[2]Department of Microbiology
[3]Department of Physics
[4]Center for Nanotechnology
The University of Washington
Seattle, Washington 98195

Summary

Surface adhesion of bacteria generally occurs in the presence of shear stress, and the lifetime of receptor bonds is expected to be shortened in the presence of external force. However, by using *Escherichia coli* expressing the lectin-like adhesin FimH and guinea pig erythrocytes in flow chamber experiments, we show that bacterial attachment to target cells switches from loose to firm upon a 10-fold increase in shear stress applied. Steered molecular dynamics simulations of tertiary structure of the FimH receptor binding domain and subsequent site-directed mutagenesis studies indicate that shear-enhancement of the FimH-receptor interactions involves extention of the interdomain linker chain under mechanical force. The ability of FimH to function as a force sensor provides a molecular mechanism for discrimination between surface-exposed and soluble receptor molecules.

Introduction

The main purpose of receptor-specific adhesion of bacteria is to prevent detachment from the target surface. In the course of infection or colonization, for example, bacteria commonly adhere to host cells or medical implants through specific adhesin-receptor interactions (Beachey, 1981; Gibbons, 1984). There they are exposed to and must resist vigorous shear stress imposed by flow of fluids such as mucosal secretions (0.8 dynes/cm^2 for saliva) or blood (up to 10 dynes/cm^2) that are presumed to act as a natural defense against bacterial colonization (Christersson et al., 1988; Dickinson et al., 1995, 1997; Pratt and Kolter, 1998; Pratt-Terpstra et al., 1987; Shive et al., 1999; Wang et al., 1995). Therefore, bacterial adhesins must be able to provide high-strength interactions with the colonizing surface under high shear conditions. One possible disadvantage, however, for a *permanently* strong binding mode could be that it would limit the ability of the attached bacteria to spread across the target surface even when shear is low. Another possible disadvantage of constitutively strong binding is that adhesins would bind soluble receptor-like inhibitors with the same high affinity as the target surface receptors. Therefore, it would be beneficial for bacteria to be able to modulate the binding strength of adhesins under variable shear. Some studies have suggested that bacteria-surface interactions might be enhanced by shear (Brooks et al., 1989; Brooks and Trust, 1983a, 1983b; Li et al., 2000; Mohamed et al., 2000). However, it has not been shown directly whether and how functional properties of bacterial adhesins are directly modulated by shear. Here, we demonstrate that shear-induced mechanical force enhances the strength of receptor-specific interactions between type 1 fimbriated *Escherichia coli* and target cells, and that this phenomenon is dependant on the structural properties of the adhesive subunit, FimH.

Type I fimbriae are a group of hair-like appendages on the bacterial surface that mediate mannose-sensitive adhesion to host cells. They are the most common type of bacterial adhesins described so far and are expressed by both commensal and pathogenic strains of enterobacteria and by some other families. In *E. coli*, type I fimbriae consist primarily of the FimA structural protein (Brinton, 1965) and terminate in a small tip structure that contains FimF, FimG, and the 30 kDa lectin-like adhesin FimH (Abraham et al., 1987; Hanson et al., 1988; Klemm and Christiansen, 1987). The FimH adhesin consists of a mannose binding lectin domain and a pilin domain that integrates FimH into the fimbrial tip (Choudhury et al., 1999). The amino acid sequence of the FimH variants expressed by different *E. coli* is on average 99% conserved, and all type 1 fimbriated *E. coli* are able to bind strongly to receptors containing trimannose structures (Sokurenko et al., 1997, 1998). At the same time, FimH adhesin of most intestinal *E. coli* strains does not mediate strong binding to receptors that contain primarily monomannose (Man1) terminal residues (Sokurenko et al., 1995, 1997, 1998). However, many FimH variants of uropathogenic *E. coli* origin have a relatively high Man1 binding capability due to the presence of functional point mutations at various positions in the FimH molecule (Schembri et al., 2000; Sokurenko et al., 1995, 1998).

Here, in order to determine whether the type 1 fimbriae interaction with target cells is modulated by shear and whether this process is mediated by FimH, we compared the ability of several structural variants of *E. coli* FimH to mediate binding to target cells under various shear conditions. We also used computer simulations of the FimH tertiary structure to understand the impact of the shear-induced mechanical stress on the adhesin's conformation.

Results and Discussion

Red Blood Cell Agglutination in Static and Dynamic Conditions

Red blood cells (RBCs) of guinea pig are the most commonly used model target cells for studying the functional properties of type 1 fimbriae. We compared the RBC-agglutinating ability of two naturally occurring FimH vari-

[5]Correspondence: evs@u.washington.edu
[6]Dr. Trintchina is visiting from the Department of Microbiology, People's Friendship University, Moscow, Russian Federation.

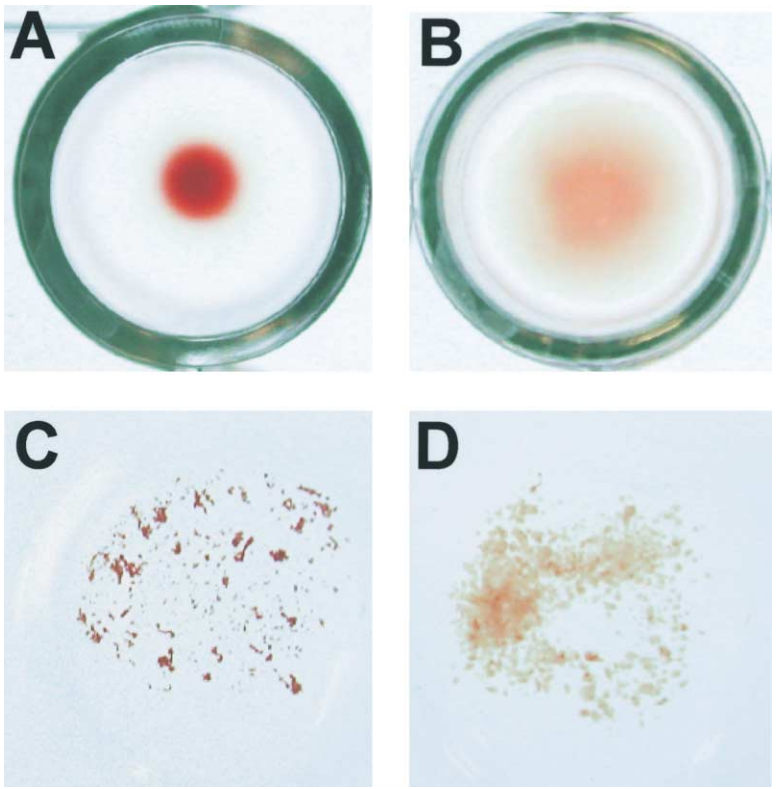

Figure 1. Agglutination of RBCs by *E. coli* in Static and Dynamic Conditions

(A) Bacteria-expressing FimH-*f18* do not form rosettes with RBC, but instead pellet to the bottom of round- bottom wells.

(B) Bacteria-expressing FimH-*j96* bind RBCs and form rosettes.

(C) When an identical mixture of FimH-*f18*-expressing bacteria and RBCs as in (A) are subjecting to rocking, they form tight aggregates.

(D) After 3 min, the aggregates in (C) have loosened.

ants—a low-Man1 binding variant, FimH-*f18*, from intestinal *E. coli* strain F18, and a variant with increased level of Man1 binding, FimH-*j96*, identical to the one expressed by uropathogenic *E. coli* strain J96 that has been crystallized (Choudhury et al., 1999). FimH-*f18* represents a structural variant that is the most common one among intestinal *E. coli*, while FimH-*j96* differs from the FimH-*f18* by A27V, S70N, and N78S substitutions (Sokurenko et al., 1995, 1998; Choudhury et al., 1999). The A27V substitution, i.e., presence of valine instead of alanine in position 27, is responsible for increased Man1 binding capability of this type of FimH (Sokurenko et al., 1995, 1997, 1998).

Two commonly used RBC agglutination assays were performed that utilize different shear conditions. Static conditions were achieved with rosette-formation assays, in which RBCs were mixed with bacteria in U-bottomed microtiter plate wells and allowed to settle undisturbed for $\sim$30 min. If no agglutination occurs, RBCs fall into a pellet in the bottom of the well (Figure 1A), while agglutination results in a rosette of RBCs crosslinked by bacteria (Figure 1B). Dynamic conditions were achieved with on-slide agglutination assays, in which the suspension of RBC and bacteria were rocked on a slide surface at $\sim$3 s^{-1}, and agglutination was indicated by clumping of RBCs by bacteria (Figure 1C).

Type 1 fimbriated bacteria expressing the FimH-*f18* variant were unable to mediate RBC agglutination in the static rosette-formation assay, even at the highest concentration of bacteria used (10^9 bacteria/ml, see Table 1A and Figure 1A). In contrast, this FimH variant was able to readily agglutinate RBCs in the dynamic rocking assay (Figure 1C), where RBCs formed tight clumps in 42 $\pm$ 3 s at the highest concentration of bacteria (10^9 bacteria/ml) and still formed aggregates when the bacteria were 10-fold diluted (Table 1A). Interestingly, however, the aggregates formed by the FimH-*f18* bacteria began to dissipate within 3 min after rocking was stopped (Figure 1D) but reformed promptly if rocking was restarted (not shown). Therefore, the FimH-*f18* variant requires dynamic conditions to agglutinate RBCs.

In contrast, bacteria expressing FimH-*j96* were able to agglutinate RBC in static conditions. This variant was able to form RBC rosettes up to an 8-fold dilution (Table 1A and Figure 1B). Under dynamic conditions, these bacteria aggregated RBCs at a slightly higher rate relative to the FimH-*f18* variant (35 $\pm$ 2 s at the highest concentration). Furthermore, the RBC aggregates induced by FimH-*j96* remained stable indefinitely long after rocking was halted (not shown).

Taken together, these results suggest that the ability of type 1 fimbriated bacteria to agglutinate RBCs depends on the shear conditions applied and that this phenomenon is mediated by specific functional properties of the FimH adhesin manifested in the FimH-*f18* variant. Importantly, expression in isogenic background of FimH variants with different Man1 binding does not affect the percentage of fimbriated bacteria, fimbriae number per bacterial cell, fimbriae morphology, or amount of FimH incorporated into the fimbriae (Sokurenko et al., 1995, 1997). In all assays, agglutination (when it occurred) was inhibitable by 50 mM α-methylmannoside, indicating its FimH-specific nature.

Shear Force-Dependent RBC Binding in Flow Chambers

To establish whether the differential pattern of RBC agglutination observed in the previous experiments is due

Table 1. FimH Mediated Man1- and Trimannose-Binding and Red Blood Cell (RBC) Agglutination under Static and Dynamic Conditions

		Receptor-binding		RBC agglutination	
	FimH variant	Man1[a]	Trimannose[b]	rosettes (static)[c]	rocking (dynamic)[d]
A	FimH-*f18*	2.0 ± 0.4	21.2 ± 2.5	>1:1	42 ± 3 sec
	FimH-*j96*	6.1 ± 0.9	20.0 ± 1.9	1:8	35 ± 2 sec
B	FimH*j96*-V27A	2.3 ± 0.5	22.0 ± 3.5	>1:1	40 ± 4 sec
C	Fimh-*f18*-V156P	4.2 ± 0.5	19.7 ± 3.0	1:8	37 ± 3 sec
	FimH-*j96*-V156P	15.5 ± 1.4	18.4 ± 2.3	1:32	33 ± 2 sec
D	FimH-*f18*-Q32L:S124A	0.4 ± 0.2	18.0 ± 1.3	>1:1	42 ± 2 sec
	FimH-*j96*-Q32L:S124A	0.5 ± 0.2	20.8 ± 2.5	>1:1	40 ± 2 sec

The binding capability of several variants of bacteria was defined as explained below. All binding was >90% inhibitable by 50 mM α-methyl-mannoside. (A) functional difference between FimH-*f18* and FimH-*j96*; (B) effect of the V27A reversion substitution in FimH-j96 on the RBC agglutination capabilities; (C) functional effects of the V156P mutation predicted to increase static binding capabilities of FimH, and (D) functional effects of the combined Q32L and S124A mutations predicted to decrease static binding capabilities of FimH.

[a] Man1 binding was measured by the number of bacteria binding to a mannosylated BSA-coated microplate under static conditions, and is expressed at 10^6 colony forming units (cfu)/well.

[b] Trimannose binding was measured by the number of bacteria binding to a bovine RNAse B-coated microplate under static conditions, and is expressed in 10^6 cfu/well.

[c] Binding to RBC in static conditions was measured as the highest dilution of bacteria that formed rosettes (1:1 is 10^9 bacteria/ml).

[d] Rate of the RBC agglutination under the dynamic, rocking conditions was measured at the highest concentration of bacteria (10^9 bacteria/ml).

to a distinct ability of shear to enhance adhesion of type 1 fimbriated bacteria to RBCs, we studied the adhesion of low- and high-Man1 binding variants to RBCs under well-defined shear conditions. Previous studies on the effect of shear on selectin- or von Willebrand factor-mediated adhesion of lymphocytes and platelets have used flow chambers (Finger et al., 1996; Marchese et al., 1999). Using a similar approach, we immobilized bacteria expressing either FimH-*f18* or FimH-*j96* on the surface of a flow chamber coated with bovine RNaseB, a model trimannose-containing receptor substrate to which both FimH variants bind with equal affinity (see Table 1A). In brief, RBCs were allowed to bind to the bacterial carpet, and the unbound cells were removed by rinsing under moderate fluid flow shear (0.28 to 0.90 dynes/cm^2). RBCs that remained attached to the bacterial carpet were then subjected to various shear conditions. As observed in the agglutination assays, the original attachment of RBCs to bacteria could be inhibited by 50 mM α-methyl-mannoside, indicating that the bacteria-RBC interactions were FimH mediated.

Under low shear conditions (from 0.01 to 0.14 dynes/cm^2 shear stress), the RBCs attached to the FimH-*f18*-expressing bacteria were found to bind weakly, such that the cells moved sporadically along the adhesive surface (Figure 2A). However, at moderate shear (0.28 to 0.90 dynes/cm^2), these RBCs exhibited decreased mobility (Figure 2D) eventually becoming firmly adhered to the FimH-*f18* bacterial carpet (Figure 2B). Not only did fewer cells move at moderate shear, but those that did moved more slowly. When the shear was switched back and forth repeatedly between low and moderate shear levels, the cells started and stopped moving repeatedly, indicating that the process of adhesion enhancement under shear was reversible. Thus, the FimH-*f18*-mediated adhesion of bacteria to RBC is stronger under moderate shear than under low shear, i.e., is shear-dependent. Furthermore, because the RBCs adhered firmly to bacteria expressing FimH-*j96* even under low shear conditions (Figure 2), the shear dependence demonstrated by the FimH-*f18* variant is an adhesin-mediated phenomenon. At sufficiently high shear (>2 dynes/cm^2), RBCs began to move on the bacteria expressing either FimH variant (Figures 2C and 2D) and at shears much higher than 10 dynes/cm^2, all RBCs detached from the bacterial carpet. Thus, the flow chamber results corresponded well to the RBC agglutination patterns, with both series of experiments indicating that FimH-*f18* mediates stronger binding of bacteria to RBCs under high shear than under low shear conditions, while bacteria expressing FimH-*j96* can bind RBCs strongly under both conditions.

Though shear force normally decreases bond lifetimes (Bell, 1978; Evans, 1999), there are at least two explanations for how shear could increase bacterial adhesion in some instances. The increased relative fluid velocities could increase the rate of FimH-receptor bond formation (i.e., have kinetics effect) as demonstrated for L-selectin-mediated rolling of leukocytes on adhesive surfaces (Alon et al., 1997; Chen and Springer, 2001). An alternative mechanism would be that the shear-induced mechanical drag force on the surface bound cell could cause a high-affinity conformation of the receptor bound adhesin and thus decrease the bond off-rate. We thus asked whether bond on-rates are increased by shear or bond off-rates are decreased by shear. While single bond kinetics measurements are beyond the scope of this paper, we have studied the off-rates for the entire RBCs from the surface. While RBCs detached from FimH-*f18 E. coli* substantially at low shear (off-rate = on average 0.1 min^{-1} at 0.2 to 0.4 dynes/cm^2), increasing shear dramatically reduced the off-rate (0.03 min^{-1} at 0.7 dynes/cm^2 and 0.002 min^{-1} at 0.14 dynes/cm^2) until it was too low to measure in our assays at shear stresses above 0.2 dynes/cm^2 because RBCs did not detach in these conditions (Figure 2E). As with the cell mobility measurements, RBC detachment rates changed with shear in a reversible manner (not shown). In addition, to distinguish whether shear *rate* (and the increase in transport kinetics, in units time^{-1}) or, alternatively, the shear *stress* (and the force on cells, in units force/area) is critical for the shear-enhanced adhesion, we adjusted

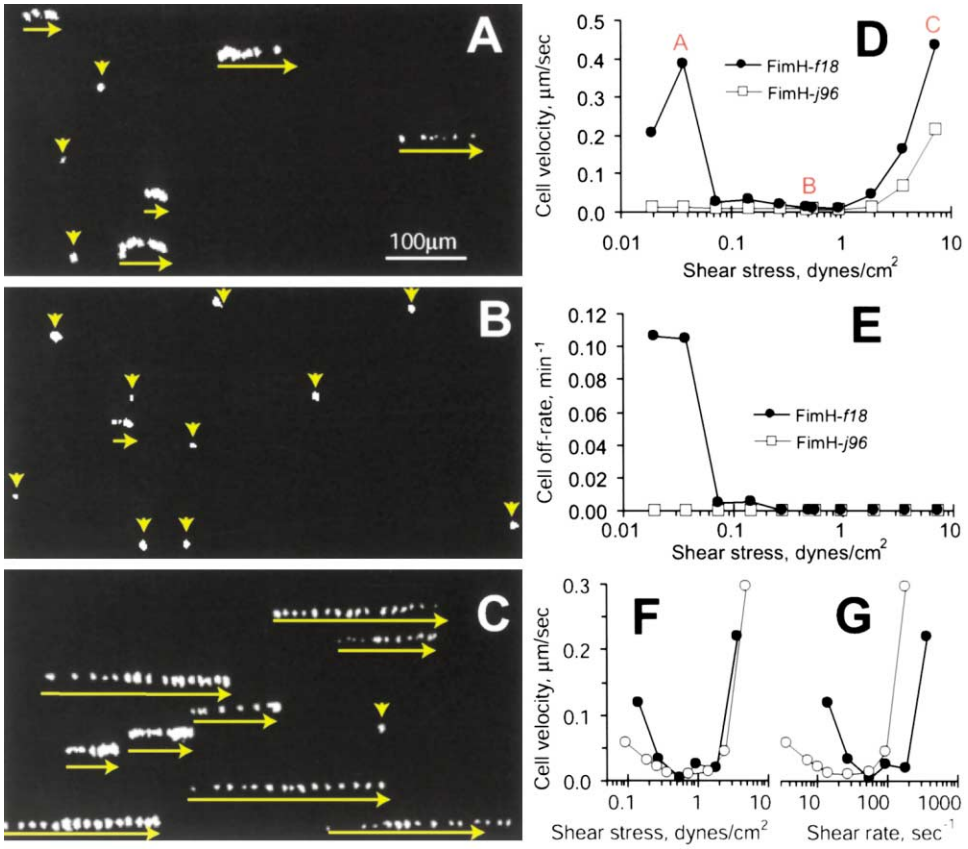

Figure 2. Movement of RBCs Bound to a Carpet of *E. coli* under Shear in a Glycotech Parallel Plate Flow Chamber

Some representative tracks of RBCs bound to FimH-*f18*-expressing *E. coli* are shown here under a shear stress of (A) 0.037 dynes/cm^2, (B) 0.55 dynes/cm^2, and (C) 7.20 dynes/cm^2 (1 dyne/cm^2 = 0.1 N/m^2 = 0.1 pN/μm^2). Each track shows 3 min total time with images taken at 10 s time intervals. The yellow arrows show the path of a single cell while surface attached, while the yellow arrowheads point to cells that did not move during the 3 min video at that shear stress. The movement at each shear was then analyzed as described in the Experimental Procedures and expressed as the average cell velocity, as shown in (D) for the low-Man1 binding FimH-*f18* (●) and the high-Man1 binding FimH-*j96* (□). Red letters in (D) indicate the shear stress values corresponding to the images in (A) through (C). Cells move the most at low or high shear stress, while cells at intermediate shear stress (0.5 dynes/cm^2) move very little. In addition to moving along the surface, some cells detached completely and moved at the fluid velocity. The rate of detachment is shown in (E) and was measurable only at low shear as cells rarely if ever detached at moderate and high shear.

(F and G) Effect of viscosity on the velocity of RBCs bound to a carpet of *E. coli*. In flow chamber experiments, RBCs were bound to *E. coli* expressing FimH-*f18* and subjected to various shears. Buffers of two different viscosities were used in order to determine whether the shear stress or shear rate was the critical determinant for increasing binding under moderate shear. The solution was calculated to have a viscosity of 1.0 centipoise (●), while addition of 6% Ficoll increased the viscosity to 2.6 centipoise (●).

(F) When average cell velocities in the two conditions were plotted against shear stress, their drop to a minimum coincided.

(G) However, when the velocities were plotted against the shear rate, the curves did not coincide. This indicates that shear stress and the force on cells, rather than shear rate and kinetic effects, mediates the effects of fluid shear on adhesion.

the viscosity of the medium in the flow chamber experiments. A solution of 6% Ficoll was used to increase the viscosity from 1.0 to 2.6 centipoise. Since shear stress is shear rate times viscosity, this should increase the shear stress and the drag forces on cells 2.6-fold without affecting the shear rate and fluid velocity. In the presence of Ficoll, RBCs were observed to bind more strongly at all shears. Moreover, they slowed down at the same shear stress with or without Ficoll, but not at the same shear rate (Figure 2F versus Figure 2G). This demonstrates that shear force and off-rates, not kinetic effects and on-rates, dominates the shear activation of the FimH-mediated adhesive interactions between RBC and the type 1 fimbriated bacteria. Therefore, the shear-enhanced adhesion of FimH occurs via a distinctly different mechanism from a previously described shear-activation of L-selectin-mediated rolling of leukocytes on the blood vessel walls (Finger et al., 1996) that is mediated by the shear rate (Chen and Springer, 2001) and by kinetic effects on selectin bond formation (Alon et al., 1997).

Prediction of Force-Induced Conformational Changes in FimH Structure

We hypothesized that the molecular mechanism of shear-dependent bacterial adhesion was based, at least in part, on the ability of the tertiary structure of receptor bound FimH to respond to the applied shear force. However, the crystal structure of FimH-*j96* cannot offer immediate insights as to how applied force could affect the tertiary structure of FimH. As mentioned above, the increased Man1 binding capability of FimH-*j96* com-

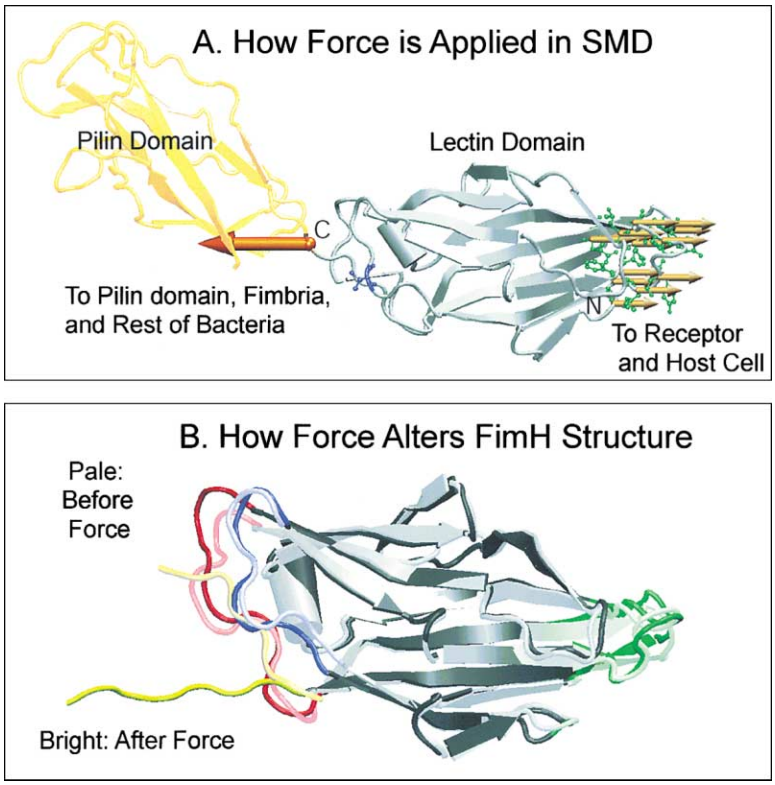

Figure 3. Steered Molecular Dynamics (SMD)

(A) shows how force is applied to the structure of FimH-*j96* (Choudhury et al., 1999). FimH consists of two domains, the pilin domain (pale gold, left) and lectin domain (gray, right). The pilin domain integrates FimH into the tip of the pilus and through it to the rest of the bacteria. It binds to and was cocrystallized with the FimC chaperone protein in the published crystal structure (Choudhury et al., 1999). The lectin domain binds the receptor and is the only structure included in the SMD simulations. The N terminus (residue F1) and C terminus (residue T158) of this domain are indicated by the letters N and C. The residues that bind the nonphysiological receptor analog in the crystal structure are shown in green ball-and-stick (residues F1, I13, N46, D47, Y48, I52, D54, Q133, N135, Y137, N138, D140, and D141). In the SMD simulations, these 13 residues are pulled with equal force in one direction (small gold arrows) while the C-α carbon of residue T158 is pulled with the same net force in the opposite direction (large gold arrow). The A27V mutation that is responsible for the increase in Man1 binding in FimH-*j96* relative to FimH-*f18* is shown in blue ball-and-stick (Sokurenko et al., 1995, 1998). (B) Comparison of the structure of the FimH lectin domain before (light) and after (dark) force is applied. The two structures were aligned to minimize rmsd of the β strands for this figure. Large changes are observed in the linker chain (yellow) to the pilin domain and to the adjoining loop regions (red and blue) to a lesser extent. However, the remainder of the protein (gray) shows only small changes, including in the receptor binding region (green). These figures were made using VMD, which was developed by the Theoretical Biophysics Group in the Beckman Institute for Advanced Science and Technology at the University of Illinois at Urbana-Champaign (Humphrey et al., 1996).

pared to FimH-*f18* is due to the presence of valine in position 27 (Sokurenko et al., 1995, 1997). The presence of valine in residue 27 also allows FimH-*j96* to agglutinate RBC in static conditions, since a recombinant FimH-*j96*-V27A with a reversion to alanine in residue 27 shows similar shear dependence of RBC agglutination as the FimH-*f18* variant (Table 1B). However, from the crystal structure of FimH-*j96* it is unclear how the A27V could affect FimH function, because this residue is located far away from the putative receptor binding site (see Figure 3A). Traditional high-resolution methods in biochemistry and biophysics, such as X-ray crystallography and NMR, can only determine equilibrium structures and structural fluctuations around equilibrium. Other methods such as atomic force microscopy, optical tweezers, and biomembrane force probes measure forces and end-to-end distances of proteins (Wang et al., 2001) or receptor bonds (Merkel et al., 1999), but cannot probe the structures at high resolution. However, a recent computational method has proven to be useful for predicting stretch-induced conformational changes with angstrom precision-steered molecular dynamics (SMD) where a known protein structure surrounded by explicit water molecules is stretched under an external force (Isralewitz et al., 2001; Vogel et al., 2001). Here, we use SMD simulations to investigate how an external force may change the FimH tertiary structure.

In order to predict force-induced conformational changes in FimH stucture, SMD simulations were performed on the crystal structure of the FimH-*j96* variant, which is the only FimH structure available at this time. Because computationally intensive simulations limit experiments to short time windows, high-level forces were used to force changes to occur at a correspondingly faster rate than in nature. Figure 3A shows that the receptor binding residues (green) are in proximity to the N terminus of the lectin domain. On the opposite side of this domain, the C terminus (residue 158) connects the lectin domain to the pilin domain and thus the rest of the fimbria and bacterium. To simulate the shear-induced tension across the lectin domain, the lectin domain was hydrated in a periodic box of water molecules, equilibrated, and subjected to force. The C terminus was pulled at a constant force in one direction while the 13 residues of the putative receptor binding site were pulled with an equivalent sum force in the opposite direction, as indicated by the gold arrows in Figure 3A. This was intended to simulate tension across the domain between the cell bound mannosyl receptor and the linkage to the pilin domain. The receptor itself was not included in the simulations because the existing crystal structure used a noncyclic substitute compound instead of a natural mannopyranose-based receptor (Choudhury et al., 1999). Similarly, we could not include the pilin domain in the simulations as it was cocrystalized with the chaperone protein (Choudhury et al., 1999), and its native conformation within the fimbial tip is unknown.

The largest change that occurred in the SMD simulations affected the amino acid chain connecting the lectin and pilin domains of FimH (Figure 3B). In the native

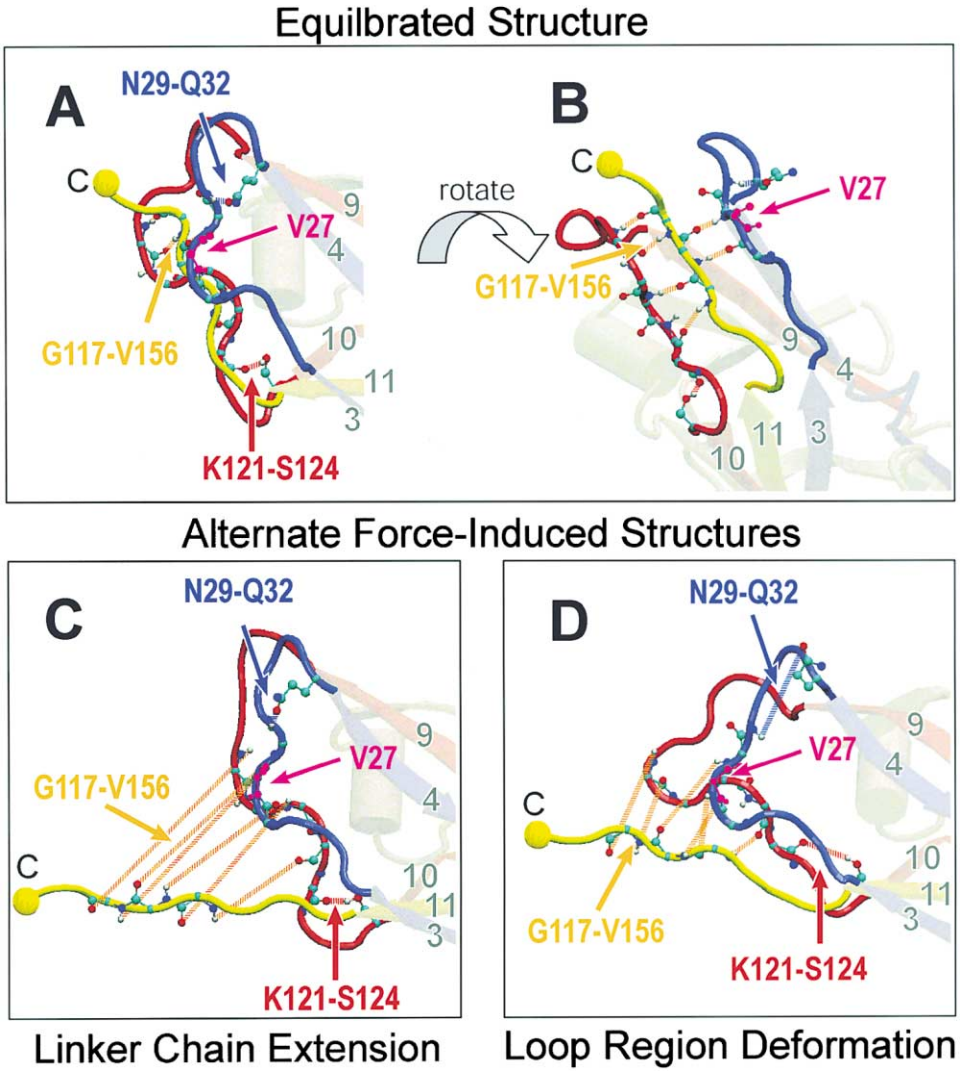

Figure 4. Structural Changes Occurring in the Interdomain Region of the FimH Lectin Domain during SMD Simulations

(A) The equilibrated structure from the viewpoint used in Figure 4. The linker chain (residues A150 to T158) is shown in yellow, the 3-4 loop in blue, and the 9-10 loop in red. Loops are identified by the β strands that they connect, and the residue and strand numbers reflect the terminology published with the crystal structure (Choudhury et al., 1999). Six hydrogen bonds that anchor the linker chain to the 3-4 and 9-10 loops in the crystal structure are shown as yellow dashed lines. A hydrogen bond between the backbone hydrogen of residue N29 and the side chain carboxyl oxygen of Q32 is shown as a blue dashed line. A hydrogen bond between the backbone oxygen of residue K121 and the side chain hydroxyl hydrogen of S124 is shown as a red dashed line The residues involved in these hydrogen bonds are shown in ball-and-stick representation, showing only the backbone atoms when the side chains are not involved in the bonds, to keep the figure cleaner. Residue V27 is shown in magenta ball and stick, and residue T128 is shown as a yellow ball at the end of the linker chain.

(B) Lateral-to-front rotation of the equilibrated structure shown in (A) offers an alternative view of the six bonds to the linker chain.

(C) One pathway that was observed to occur upon application of force was linker chain extension. Shown here is a typical conformation resulting from linker chain extension, from the same viewpoint as in (A).

(D) In some simulations, an alternative pathway was observed in which the N29-Q32 (blue arrow) and/or K121-S124 (red arrow) side chain hydrogen bonds broke, the 3-4 and 9-10 loops distorted, and the linker chain separated more slowly from the loop regions if at all. Shown here is a typical conformation resulting from loop region deformation, from the same viewpoint as in (A). These figures were made using VMD, which was developed by the Theoretical Biophysics Group in the Beckman Institute for Advanced Science and Technology at the University of Illinois at Urbana-Champaign (Humphrey et al., 1996).

structure, the interdomain linker chain consisted of 157–159 PTG amino acids (Choudhury et al., 1999), while the 154–156 VVV residues of the lectin domain are stabilized by hydrogen bonds with residues 117–120 GVAI of the 9-10 loop and residues 26–28 PVV in the 3-4 loop (Figures 4A and 4B). In the simulations, the external force caused these hydrogen bonds to break (Figure 4C) and residues 154 to 156 to pull away from the rest of the lectin domain, doubling the length of the linker chain that connects the lectin and pilin domains (Figure 4A versus Figure 4C). This change was observed in multiple simulations carried out at a constant force of 700 pN or above. In contrast to the interface region, the rmsd changes that occurred in the main β sheets of the FimH

lectin domain upon application of force (1.1 Å, Figure 3B) were comparable to the fluctuations that occurred during equilibration (0.9 Å).

Remarkably, the A27V substitution in FimH-*j96* is located in this region of linker-stabilizing bonds (see Figure 4), which were predicted by the SMD simulations to play a critical role in the force-induced conformational changes in FimH, suggesting that the linker extension might be a functionally relevant event. However, it is important to note here that force-induced linker chain extension would lead to other structural events in the FimH molecule. Specifically, it would eliminate contacts between the FimH lectin domain and the FimH pilin domain or other fimbrial subunits. These additional changes may not be observable in SMD simulations if they involve other domains for which suitable crystal structures are not available. Because the linker chain is likely to be only one step in a cascade of force-induced conformational changes, the A27V substitution that affects shear-modulated properties of FimH may either alter the extension of the linker chain itself or, alternatively, may affect other steps in this cascade. We discuss the possibility below that, beside A27V, many other mutations of similar location may also affect the receptor binding properties of FimH under various shear conditions. While elucidation of any additional events or the role of different structural mutations in these events is beyond the scope of this work, it should be possible to test the importance of linker chain extension by engineering mutations in FimH that are predicted to affect this event and testing them in functional assays.

Experimental Tests of the SMD Predictions

If the linker chain extension is indeed critical to the shear-enhanced adhesion, then structural mutations that allow the linker chain to extend more easily should result in a FimH variant that requires lower shear to enhance bacterial adhesion. According to the SMD simulations described above, reduction of the force required to switch the linker conformation should be achieved by eliminating the stabilizing bonds between residues 154–156 VVV in the linker chain and the surrounding loop regions. Each of the stabilizing bonds is a backbone hydrogen bond and can be eliminated by replacing the hydrogen-donating residue with a proline. The latter has a closed ring structure that lacks the nitrogen-associated hydrogen atom in the backbone. To determine whether elimination of linker-chain stabilizing hydrogen bonds would affect the pattern of shear-dependent *E. coli* binding to RBCs, we engineered the point mutations V154P, V155P, and V156P into the FimH-*j96* and FimH-*f18* variants and tested their binding to RBCs. For all three mutations, the trimannose binding function was entirely conserved (Table 1C and not shown), suggesting that they did not cause major structural changes in FimH. For both FimH-*j96* and FimH-*f18* variants, the most dramatic functional change was observed with a V156P mutant (Table 1C). This is the outermost residue of the anchored stretch of the linker chain and the bond destroyed by this mutation is the outermost bond of the three force-bearing bonds. Both FimH-*f18*-V156P and FimH-*j96*-V156P mutants were able to agglutinate RBCs in static conditions significantly better than the corresponding wild-types into which the mutations were introduced (Table 1C). In flow chamber experiments, FimH-*f18*-V156P mediated a dramatically stronger adhesion under low shear than did the FimH-*f18* parent (Figure 5A). Therefore, experimental evidence supports our prediction that eliminating hydrogen bonds critical to the linker chain extension will reduce the amount of shear needed to enhance adhesion of FimH to RBCs.

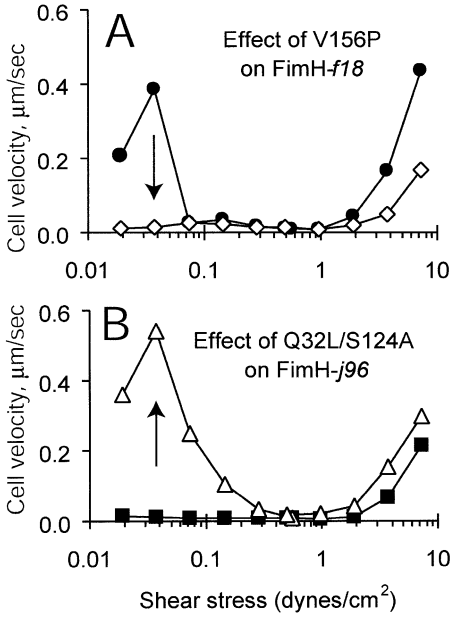

Figure 5. Effect of FimH Mutations on the Velocity of RBCs Bound to a Carpet *of E. coli*

Reduction of the velocity of surface bound RBCs reflects enhanced adhesion.

(A) In flow chamber experiments, RBCs on bacteria expressing FimH-*f18* with the V156P mutation in the linker chain (◇) moved less under low shear stress than did those on FimH-*f18* (●). Thus, as predicted by SMD, this mutation decreased the amount of force needed to increase adhesion due to a partial destabilization of the linker chain of FimH-*f18*.

(B) RBCs on bacteria expressing FimH-*j96* with the Q32L/S124A mutations in the loop regions near the linker chain (Δ) moved much more under low shear stress than those on FimH-*j96* (■). This is consistent with the SMD prediction that this mutation would increase the force needed to activate adhesion, due to a partial stabilization of the linker chain of FimH-*j96*. Experiments were performed and analyzed as in Figure 2.

To further test the hypothesis that the force-induced linker chain extension leads to stronger binding under shear, we used SMD simulations to design a mutant with the linker chain stabilized against extension. The goal was to determine whether such a mutant would require more force to enhance FimH adhesion, i.e., would have the opposite effect from the putative extension-facilitating mutation V156P. We concluded that we could not build a stabilizing disulfide bond into the linker chain without altering the native structure, because no residue pairs were properly positioned for this (determined by the MODIPY program [Sowdhamini et al., 1989]). However, SMD simulations predicted that we could indirectly stabilize the linker chain. In some SMD simulations, an alternative force response was observed

that correlated with delayed linker chain extension, so that the structure seen in Figure 4D was observed instead of that in Figure 4C. Two hydrogen bonds spanning turns in the 3-4 and the 9-10 linker-stabilizing loops ruptured (red and blue arrows, Figure 4A versus Figure 4D), and one or both loops distorted and extended along with the linker chain, instead of separating from it (Figure 4D, red and blue loops). If these SMD observations were correct, FimH lacking these two hydrogen bonds would require more force to switch the linker chain conformation and consequently to enhance adhesion. We thus made two mutations, Q32L and S124A, in the structure of both FimH variants. As expected, the most dramatic functional effect of the mutations was evident in the background of FimH-*j96* variant that binds RBCs strongly under static conditions. In support of our hypothesis, each mutation individually (not shown) and, especially together (Table 1D), eliminated the ability of the bacteria to agglutinate RBCs under static conditions. In the flow chamber experiments, the double mutant mediated a dramatically reduced adhesion at low shear relative to the FimH-*j96* variant, but provided comparable attachment to RBCs at medium and high shear, thus showing shear enhancement (Figure 5B). This is all consistent with the prediction that these mutations would increase the force needed to induce the linker chain extension and thereby increase the adhesive strength.

The three assays used in this work—Man1or trimannose receptor binding, RBC agglutination assays, and the flow chambers experiments—have different dependencies on binding kinetics. Nevertheless, when introduced into either FimH-*f18* or FimH-*j96*, the V156P mutation increased Man1 and low-shear binding, while the Q32L/S124A decreased Man1and low-shear binding in all three assay types. Therefore, our hypothesis that the linker chain between the lectin and pilin domains extends and leads to activation of bacteria-cell adhesion has generated two separate predictions that were experimentally verified here using structural mutations and the three functional assays.

Functional Significance of Shear-Enhanced Adhesion

In addition to altering the shear dependence of RBC adhesion, the mutations tested above affected the affinity of FimH for Man1 receptors. The V156P substitution increased Man1 affinity when introduced into both FimH variants, while the Q32L/S124A substitutions decreased Man1 binding of both FimH-*j96* and FimH-*f18* to an almost undetectable level (Table 1, C and D). Neither mutation affected FimH trimannose binding (Table 1, C and D). Importantly, the Man1 binding capability of all FimH variants tested correlated directly with their ability to agglutinate RBCs under static conditions (Figure 6A). Furthermore, in addition to the A27V substitution, other naturally occurring mutations as well as some induced mutations that enhance Man1 binding to varying degrees also correspondingly enhance RBC agglutination in static conditions (Sokurenko et al., 1998, 2001). Remarkably, some of the Man1-enhancing mutations identified previously (e.g., A25P, A118V, and the 117G-120I deletion) are located within or immediately adjacent to

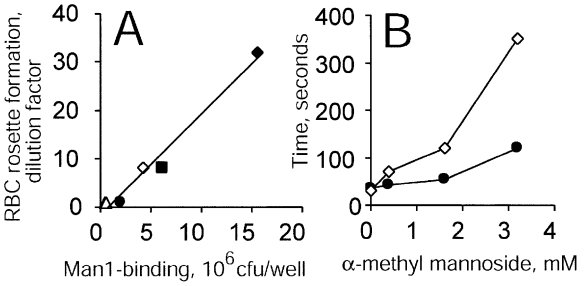

Figure 6. Functional Significance of Shear Activation

(A) Correlation between the ability of recombinant *E. coli* strains to agglutinate RBCs in static conditions and to bind Man1 receptors (see Table 1).

(B) Effect of α-methyl-mannoside on the aggregation of RBC by *E. coli* bacteria expressing either FimH-*f18* variant (●) or FimH-*f18*-V156P mutant (◇) under dynamic conditions as described in Table 1.

the region of linker-stabilizing bonds, while most of the remaining functional mutations map to the interdomain region of the lectin as well as the pilin domain of FimH (Schembri et al., 2000, Sokurenko et al., 2001). These mutations might therefore affect different steps in the force-induced conformational changes discussed above. Taken together, the studies presented here and those described previously suggest that the change in the affinity toward Man1 and the shear dependence of FimH are concurrent processes.

There are at least two mechanisms that could explain how force- and/or mutation-induced structural changes in the linker chain region could enhance binding to a cellular receptor. First, conformational changes in the interface between the pilin and lectin domains could propagate across the lectin domain and cause the receptor binding site to change from a "low-affinity" to a "high-affinity" receptor binding conformation. This mechanism has been suggested for the platelet binding protein, von Willebrand Factor, in which crystal structures showed how a remote point mutation causes a cascade of structural changes reaching to the distant receptor binding site (Celikel et al., 2000). Here, however, additional knowledge of the nature of the RBC receptor recognized by FimH and the crystal structure of the FimH-receptor bond would be required to address a possibility for such a mechanism. A second mechanism for shear activation is that the force-induced conformational change in the linker chain region of FimH might expose an additional "cryptic" binding site, not yet identified in the crystal structure. Therefore, future research will be needed to reveal the exact molecular mechanism of the adhesion enhancement by shear.

The low-Man1 binding, shear-dependent FimH variants are predominant among *E. coli*. One possible advantage for shear-dependent binding is that it might allow bacteria to attach to the colonizing surface under high shear, yet be able to move and spread across the surface by transient detaching or rolling under low shear. Another possible advantage stems from the fact that, under shear, the drag force on a surface bound bacteria is substantial, while the drag force on soluble low-molecular weight molecules is negligible. If force in-

creases adhesion, then shear will favor binding of surface-immobilized receptors over inhibition by soluble molecules. Thus, shear-activated adhesion could provide a mechanism for bacteria to resist, at least to a certain extent, soluble inhibitors that would otherwise be effective in blocking adhesion. We examined how the ability of FimH to respond to shear influenced its susceptibility to inhibitors in dynamic conditions. We compared the aggregation of RBC by the FimH-*f18*-V156P mutant to that of the wild-type FimH-*f18* under various concentrations of α-methyl mannoside, a competitive inhibitor of FimH adhesion. Wild-type FimH-*f18* mediated RBC aggregation at a slightly slower rate than the mutant in the absence of inhibitors, but at a much higher rate than the mutant in the presence of inhibitors (Figure 6B). Thus, the dependence of wild-type FimH-*f18* on shear correlates with increased resistance to inhibition under shear. Under certain circumstances, therefore, the shear-dependent mode of adhesion could provide a considerable adaptive edge. For example, the physiological role of type 1 fimbriated *E. coli* of intestinal origin is a transient colonization of the oropharyngeal epithelium that might be necessary for a successful bacterial passage through the stomach barrier and spread into the intestine (Bloch et al., 1992). On the oropharyngeal mucosa, the bacteria are subjected to high shear created by saliva and food swallowing movements, concomitantly with a high concentration of soluble highly mannosylated compounds in the saliva. On the other hand, the FimH-*j96* that demonstrated the shear-independent mode of adhesion is a naturally occurring variant and the high-Man1 binding FimH variants are typical of uropathogenic strains. The shear-independent mode of bacterial adhesion could be more advantageous for a fast massive colonization of surfaces irrespectively to the shear present and in the presence of a relatively low concentration of soluble mannosylated compounds, e.g., in the course of colonization of urinary bladder epithelium or renal tissue compartments. Natural occurrence of such variants, therefore, could reflect an ongoing adaptive molecular evolution of the *E. coli* to yield a binding mechanism that is alternative to the predominant shear-dependent one. Thus, it will be interesting to define selective advantage of the different FimH binding modes using various animal models of *E. coli* infection.

Although we only report on the *E. coli* adhesion, FimH is the most common type of bacterial adhesin known (most species of enterobacteria and vibrio possess it), so shear-activated adhesion may prove to be the norm rather than an exception. Moreover, the shear-activated mode of adhesion is unlikely to be limited to FimH. Shear has been shown to increase the binding of *Staphylococcus aureus* bacteria to certain collagen receptors (Li et al., 2000; Mohamed et al., 2000), and the advantages of shear-activated adhesion to bacteria are as universal as is the presence of shear flow. Extending beyond bacteria, shear-activated adhesion could be a common phenomenon in viral infection and in mammalian cell-cell or cell-surface interactions involved in various functions. The fact that receptor-adhesin interactions can be activated by mechanical force highlights an additional dimension for how physiological factors are able to modulate the functional properties of proteins. With the help of computer simulations and nanotechnology tools, we should gain insights into the structural mechanisms by which proteins can act as force sensors and undergo a functional switch when subjected to mechanical force in vivo. This information is crucial for understanding the underlying mechanisms of cell surface adhesive interactions and has the potential to be exploited for medical and technological applications.

Experimental Procedures

Reagents

Monomannosylated BSA (Man1-BSA) was obtained from EY Laboratories, Inc. (San Mateo, CA). Guinea pig red blood cells (RBCs) were purchased from Colorado Serum Co. (Denver, CO). All other reagents were obtained from Sigma (St. Louis, MO).

Bacterial Strains and Plasmids

Recombinant strains utilized here were constructed using a *fim* null K-12 derivative, AAEC191A (provided by Dr. Ian Blomfield, University of Kent, UK), and were described previously (Sokurenko et al., 1995). AAEC191A was transformed with the recombinant plasmid pPKL114 (provided by Dr. Per Klemm, Danish Technical University, Copenhagen, Denmark) to create strain KB18. Plasmid pPKL114 is a pBR322 derivative containing the entire *fim* gene cluster from the *E. coli* K-12 strain, PC31, but with a translational stop-linker inserted into the unique KpnI site of the *fimH* gene. Strain KB18 cells express no fimbriae or very few numbers of long, nonadhesive fimbriae. For the studies reported here, strain KB18 was cotransformed with a series of isogenic pGB2-24-based plasmids. Plasmid pGB2-24 is a pACYC184 derivative used for expression of various *fimH* alleles under *bla* promoter. Recombinant strains created using these plasmids express large numbers of fully functional and morphologically identical type 1 fimbriae. Site-directed mutagenesis was performed essentially as described previously (Beck and Burtscher, 1994).

Binding Assays

Assays of bacterial adhesion to Man1-BSA and bovine RNAseB immobilized in 96-well plates were carried out as described previously (Sokurenko et al., 1995). Briefly, Man1-BSA and bovine RNAseB were dissolved at 20 μg/ml in 0.02 M bicarbonate buffer, and 100 μl aliquots were incubated in microtiter wells for 1 hr at 37°C. The wells were then washed three times with PBS and quenched with 0.1% BSA in PBS. ^{3}H-thymidine-labeled bacteria were added in 0.1% BSA in PBS and incubated for 40 min at 37°C without shaking to achieve saturation, and the wells were then washed with PBS. The individual wells were subjected to scintillation counting. The density of bacteria used in all assays was 5×10^7 colony forming units per 100 μl. RBC rosette-formation assay was performed by mixing equal amounts of serially diluted bacterial suspensions (starting from OD_{540} nm = 1.0) and a 1% suspension of RBC in U-bottom microtiter plate wells. On-slide agglutination assays was performed by mixing the suspension of RBC and bacteria on a slide surface followed by rocking at $\sim$3 s^{-1}.

Parallel Plate Flow Chamber Experiments

Bacteria-coated dishes were prepared as follows: 35 mm tissue culture dishes were incubated with 20 μg/ml RNAse B in 0.02 M bicarbonate buffer for 1 hr at 37°C and washed three times in PBS with 0.1% BSA (PBS-BSA). The dishes were then incubated with 200 μl PBS-BSA containing 10^8 colony-forming units of *E. coli* for 1 hr at 37°C and washed three times. The *E. coli* bound through interaction of FimH with RNAse B (see Table 1) and FimH-negative bacteria did not bind significantly to the dishes (not shown). In all other variants, the *E. coli* were observed to form a confluent carpet of bacteria after this treatment, which was not perceptibly altered during the course of the flow chamber experiments. The dishes were then placed under a Glycotech parallel plate flow chamber with a size B gasket (2.5 cm $\times$ 0.25 cm $\times$ 250 μm) and sealed with vacuum. A Harvard model #975 pulse-free syringe pump was used to pump fluid through the chamber. The dishes were equilibrated in the flow chamber with PBS-BSA, and a 0.1% solution of RBC was injected into the chamber, allowed to settle onto the bacterial

carpet, and washed with PBS-BSA at a shear stress of about 0.5 dynes/cm^2 until all free cells had been removed from the chamber and upstream tubing. The volumetric flow was then reduced to bring the shear stress down to 0.01–0.02 dynes/cm^2, and the shear stress was stepped up 2-fold, with at least 3 min at each shear stress.

RBC movement was recorded using phase contrast microscopy with a 20× objective, a CCD camera, and Metamorph video imaging software by Universal Imaging. Videos were recorded at 1 frame every 2 s for a total of 3 min at each shear rate. The position of each RBC was tracked at 6 s intervals in these videos using Metamorph's point tracking plug-in. The average velocity for each cell was calculated from these positions over the 3 min at each shear. These were then averaged for the average velocity of all cells. Some cells detached completely at the low shear stress and moved at the fluid velocity. (A cell moving in flow near a surface has velocity approximately equal to the cell radius, 5 μm, times the shear rate, assuming it is almost touching the surface.) Since these times reflected movement without any bond detachment, these time intervals were removed from the analysis for each cell. We only analyzed cells that were attached and in the field of view at the start of the 3 min time frame. The off-rate of RBCs was calculated from the X, the percent of original RBCs remaining bound at time t, using the formula $k = 1/t \cdot ln(1/X)$, and using $t = 3$ min. This assumes that detachment is independent and governed by a single rate constant, and $X = e^{-kt}$, so that the number of remaining RBCs decays exponentially.

Steered Molecular Dynamics

Steered molecular dynamics simulations were performed using NAMD 2.3, which was developed by the Theoretical Biophysics Group in the Beckman Institute for Advanced Science and Technology at the University of Illinois at Urbana-Champaign (Kale et al., 1999). Molecular dynamics was performed as described earlier (Krammer et al., 2002), except that particle mesh ewald summations were used to calculate electrostatic contributions beyond the 13 Å cut-off. In brief, the lectin domain of FimH (residues F1 to T158) was hydrated in a 54 × 54 × 100 Å^3 periodic box of water molecules and equilibrated for at least 500 ps. For equilibration and the ensuing simulations under force, the system was coupled to a 310 K bath and was coupled anisotropically to a Berendson pressure piston set at one bar with a relation time of 1 ps and a compressibility factor of 4.5×10^{-5} bar. During the equilibration, the box relaxed to 51.6 × 51.6 × 95.6 Å^3 and remained the same size within 0.3% during simulations. When hydrogen atoms were added to the crystal structure, a disulfide bond was assumed between residues C3 and C44, and residue H45 was assumed to be protonated because it was surrounded by negatively charged residues D47 and D100 in the crystal structure (Choudhury et al., 1999). This left a net zero charge in the system as required for particle mesh ewald.

To simulate the shear-induced tension between the cell bound receptor and the anchor from the lectin domain to the pilin domain, the C terminus of the lectin domain was pulled at a constant force in one direction while the 13 residues of the putative receptor binding site were pulled with an equivalent sum force in the opposite direction. Forces were applied to the C-α carbon of each residue and the receptor binding residues were assumed to be the 13 residues that interacted with the C-HEGA mannose analog in the crystal structure (residues F1, I13, N46, D47, Y48, I52, D54, Q133, N135, Y137, N138, D140, and D141). Each run lasted about 1000 ps, and the total force ranged between 600 and 1000 pN, with at least two runs at each force, where each run at the same force used starting structures from different times during equilibration. Each run contained 26,892 atoms and required 4 days of simulation time on a Scyld linux beowulf cluster with 12 nodes running at 1.3 GHz for the 1 to 2 ns required.

Acknowledgments

We would like to thank Dr. Klaus Schulten and his research group for valuable advice and training in SMD, and David Craig for his many contributions and fruitful discussions. We also thank Drs. Steve Moseley, Oleg Prezhdo, Yuriy Pereverzev, Colin Manoil, Kelly Hughes, James Champoux, Heidrun Interthal, and Gretchen Baneyx for valuable discussions and/or suggestions on improving the quality of manuscript. E.V.S. would like to express gratitude to the late Dr. J. Ronald Doyle for his inspiring encouragement of this work. The research was supported by the National Institutes of Health grants R01 AI45820 and P01 DK53369 (E.V.S.), the NIH NHGRI Center of Excellence in Genomic Science grant number 1 P50 HG02360-01(V.V.), NIH grant 5R01 GM49063 (V.V.), a Whitaker Foundation Graduate Fellowship (W.E.T.), and a National Computational Science Alliance grant MCB000010N utilizing the Origin2000 machine (V.V.).

Received: March 21, 2002
Revised: May 21, 2002

References

Abraham, S.N., Goguen, J.D., Sun, D., Klemm, P., and Beachey, E.H. (1987). Identification of two ancillary subunits of *Escherichia coli* type 1 fimbriae by using antibodies against synthetic oligopeptides of *fim* gene products. J. Bacteriol. *169*, 5530–5536.

Alon, R., Chen, S., Puri, K.D., Finger, E.B., and Springer, T.A. (1997). The kinetics of L-selectin tethers and the mechanics of selectin-mediated rolling. J. Cell Biol. *138*, 1169–1180.

Beachey, E.H. (1981). Bacterial adherence: adhesin-receptor interactions mediating the attachment of bacteria to mucosal surface. J. Infect. Dis. *143*, 325–345.

Beck, R., and Burtscher, H. (1994). Introduction of arbitrary sequences into genes by use of class IIs restriction enzymes. Nucleic Acids Res. *22*, 886–887.

Bell, G.I. (1978). Models for the specific adhesion of cells to cells. Science *200*, 618–627.

Bloch, C.A., Stocker, B.A., and Orndorff, P.E. (1992). A key role for type 1 pili in enterobacterial communicability. Mol. Microbiol. *6*, 697–701.

Brinton, C. (1965). The structure, function, synthesis and genetic control of bacterial pili and a molecular model for DNA and RNA transport in gram-negative bacteria. Trans. N. Y. Acad. Sci. *27*, 1003–1054.

Brooks, D.E., and Trust, T.J. (1983a). Enhancement of bacterial adhesion by shear forces: characterization of the haemagglutination induced by *Aeromonas salmonicida* strain 438. J. Gen. Microbiol. *129*, 3661–3669.

Brooks, D.E., and Trust, T.J. (1983b). Interactions of erythrocytes with bacteria under shear. Ann. N Y Acad. Sci. *416*, 319–331.

Brooks, D.E., Cavanagh, J., Jayroe, D., Janzen, J., Snoek, R., and Trust, T.J. (1989). Involvement of the MN blood group antigen in shear-enhanced hemagglutination induced by the *Escherichia coli* F41 adhesin. Infect. Immun. *57*, 377–383.

Celikel, R., Ruggeri, Z.M., and Varughese, K.I. (2000). von Willebrand factor conformation and adhesive function is modulated by an internalized water molecule. Nat. Struct. Biol. *7*, 881–884.

Chen, S., and Springer, T.A. (2001). Selectin receptor-ligand bonds: formation limited by shear rate and dissociation governed by the Bell model. Proc. Natl. Acad. Sci. USA *98*, 950–955.

Choudhury, D., Thompson, A., Stojanoff, V., Langermann, S., Pinkner, J., Hultgren, S.J., and Knight, S.D. (1999). X-ray structure of the FimC-FimH chaperone-adhesin complex from uropathogenic *Escherichia coli*. Science *285*, 1061–1066.

Christersson, C.E., Glantz, P.O., and Baier, R.E. (1988). Role of temperature and shear forces on microbial detachment. Scand. J. Dent. Res. *96*, 91–98.

Dickinson, R.B., Nagel, J.A., McDevitt, D., Foster, T.J., Proctor, R.A., and Cooper, S.L. (1995). Quantitative comparison of clumping factor- and coagulase-mediated *Staphylococcus aureus* adhesion to surface-bound fibrinogen under flow. Infect. Immun. *63*, 3143–3150.

Dickinson, R.B., Nagel, J.A., Proctor, R.A., and Cooper, S.L. (1997). Quantitative comparison of shear-dependent *Staphylococcus aureus* adhesion to three polyurethane ionomer analogs with distinct surface properties. J. Biomed. Mater. Res. *36*, 152–162.

Evans, E. (1999). Looking inside molecular bonds at biological interfaces with dynamic force spectroscopy. Biophys. Chem. *82*, 83–97.

Finger, E.B., Puri, K.D., Alon, R., Lawrence, M.B., von Andrian, U.H., and Springer, T.A. (1996). Adhesion through L-selectin requires a threshold hydrodynamic shear. Nature *379*, 266–269.

Gibbons, R.J. (1984). Adherent interactions which may affect microbial ecology in the mouth. J. Dent. Res. *63*, 378–385.

Hanson, M.S., Hempel, J., and Brinton, C.C. (1988). Purification of the *Escherichia coli* type 1 pilin and minor pilus proteins and partial characterization of the adhesin protein. J. Bacteriol. *170*, 3350–3358.

Humphrey, W., Dalke, A., and Schulten, K. (1996). VMD: visual molecular dynamics. J. Mol. Graph. *14*, 33-8, 27-8.

Isralewitz, B., Gao, M., and Schulten, K. (2001). Steered molecular dynamics and mechanical functions of proteins. Curr. Opin. Struct. Biol. *11*, 224–230.

Kale, L., Skeel, R., Bhandarkar, M., Brunner, R., Gursoy, A., Krawetz, N., Phillips, J., Shinozaki, A., Varadarajan, K., and Schulten, K. (1999). NAMD2: greater scalability for parallel molecular dynamics. J. Comput. Phys. *151*, 283–312.

Klemm, P., and Christiansen, G. (1987). Three *fim* genes required for the regulation of length and mediation of adhesion of *Escherichia coli* type 1 fimbriae. Mol. Gen. Genet. *208*, 439–445.

Krammer, A., Craig, D., Thomas, W.E., Schulten, K., and Vogel, V. (2002). A structural model for force regulated integrin binding to fibronectin's RGD-synergy site. Matrix Biol. *21*, 139–147.

Li, Z.J., Mohamed, N., and Ross, J.M. (2000). Shear stress affects the kinetics of *Staphylococcus aureus* adhesion to collagen. Biotechnol. Prog. *16*, 1086–1090.

Marchese, P., Saldivar, E., Ware, J., and Ruggeri, Z.M. (1999). Adhesive properties of the isolated amino-terminal domain of platelet glycoprotein Ibalpha in a flow field. Proc. Natl. Acad. Sci. USA *96*, 7837–7842.

Merkel, R., Nassoy, P., Leung, A., Ritchie, K., and Evans, E. (1999). Energy landscapes of receptor-ligand bonds explored with dynamic force spectroscopy. Nature *397*, 50–53.

Mohamed, N., Rainier, T.R., and Ross, J.M. (2000). Novel experimental study of receptor-mediated bacterial adhesion under the influence of fluid shear. Biotechnol. Bioeng. *68*, 628–636.

Pratt, L.A., and Kolter, R. (1998). Genetic analysis of *Escherichia coli* biofilm formation: roles of flagella, motility, chemotaxis and type I pili. Mol. Microbiol. *30*, 285–293.

Pratt-Terpstra, I.H., Weerkamp, A.H., and Busscher, H.J. (1987). Adhesion of oral streptococci from a flowing suspension to uncoated and albumin-coated surfaces. J. Gen. Microbiol. *133*, 3199–3206.

Schembri, M.A., Sokurenko, E.V., and Klemm, P. (2000). Functional flexibility of the FimH adhesin: insights from a random mutant library. Infect. Immun. *68*, 2638–2646.

Shive, M.S., Hasan, S.M., and Anderson, J.M. (1999). Shear stress effects on bacterial adhesion, leukocyte adhesion, and leukocyte oxidative capacity on a polyetherurethane. J. Biomed. Mater. Res. *46*, 511–519.

Sokurenko, E.V., Courtney, H.S., Maslow, J., Siitonen, A., and Hasty, D.L. (1995). Quantitative differences in adhesiveness of type 1 fimbriated *Escherichia coli* due to structural differences in fimH genes. J. Bacteriol. *177*, 3680–3686.

Sokurenko, E.V., Chesnokova, V., Doyle, R.J., and Hasty, D.L. (1997). Diversity of the *Escherichia coli* type 1 fimbrial lectin. Differential binding to mannosides and uroepithelial cells. J. Biol. Chem. *272*, 17880–17886.

Sokurenko, E.V., Chesnokova, V., Dykhuizen, D.E., Ofek, I., Wu, X.R., Krogfelt, K.A., Struve, C., Schembri, M.A., and Hasty, D.L. (1998). Pathogenic adaptation of *Escherichia coli* by natural variation of the FimH adhesin. Proc. Natl. Acad. Sci. USA *95*, 8922–8926.

Sokurenko, E.V., Schembri, M.A., Trintchina, E., Kjaergaard, K., Hasty, D.L., and Klemm, P. (2001). Valency conversion in the type 1 fimbrial adhesin of *Escherichia coli*. Mol. Microbiol. *41*, 675–686.

Sowdhamini, R., Srinivasan, N., Shoichet, B., Santi, D.V., Ramakrishnan, C., and Balaram, P. (1989). Stereochemical modeling of disulfide bridges. Criteria for introduction into proteins by site-directed mutagenesis. Protein Eng. *3*, 95–103.

Vogel, V., Thomas, W.E., Craig, D.W., Krammer, A., and Baneyx, G. (2001). Structural insights into the mechanical regulation of molecular recognition sites. Trends Biotechnol. *19*, 416–423.

Wang, I.W., Anderson, J.M., Jacobs, M.R., and Marchant, R.E. (1995). Adhesion of *Staphylococcus epidermidis* to biomedical polymers: contributions of surface thermodynamics and hemodynamic shear conditions. J. Biomed. Mater. Res. *29*, 485–493.

Wang, K., Forbes, J.G., and Jin, A.J. (2001). Single molecule measurements of titin elasticity. Prog. Biophys. Mol. Biol. *77*, 1–44.